# Multicomponent processing of seismic data at the Jackfish Heavy Oil Project, Alberta

Karen J. Pengelly, Larry R. Lines, and Don C. Lawton


## ABSTRACT

This investigation was undertaken to evaluate the processing flows needed to obtain vertical and radial post-stack migrated seismic sections from a heavy oil reservoir in Eastern Alberta. The radial filter was found to successfully attenuate shot-generated linear noise on both the vertical and radial components. Gabor deconvolution was found to successfully boost signal to noise in low fold areas of the data. The depth-variant stack has shown to have greater frequency in the near surface data compared to the CCP stack for the radial component.


## INTRODUCTION

This investigation was undertaken to evaluate the processing flows needed to obtain vertical and radial post-stack migrated seismic sections from a heavy oil reservoir in Eastern Alberta. Converted-wave seismic processing flows have been previously investigated and documented by Harrison (1992) and Isaac (1996). Of particular importance to converted-wave processing is the analysis of receiver statics. Isaac (1996) and Cary and Eaton (1993) showed that S-wave receiver statics can be extremely large and variable compared to P-wave receiver statics. It is not uncommon to have S-wave receiver statics on the order of +/- 200 ms, whereas P-wave receiver statics are commonly small, usually under 20 ms.

Velocity analysis is an integral component of converted-wave processing. There has been extensive research relating to nonhyperbolic moveout, valid for weak anisotropy. In many cases, for short to medium offset P-P data, hyperbolic NMO is an adequate approximation for moveout used in velocity estimations (Al-Chalabi, 1973; Tsvankin and Thomsen, 1994; Alkhalifah, 1997). For PS data, the hyperbolic NMO correction is valid only for short offsets (Iverson, et al., 1989). Furthermore, Castagna and Chen (2000) found that conventional processing software assumes hyperbolic moveout and may produce false structure and false responses below anisotropic regions because of improper removal of NMO. It has been found that the overlying rock in some heavy oil areas exhibit high values of anisotropy. Newrick and Lawton (2003) found that at Pikes Peak, Saskatchewan, the Thomsen parameters of anisotropy have values of $\varepsilon$=0.12 +/- 0.02 and $\delta$=0.30 +/- 0.06, from data using a multi-offset VSP. If the Jackfish area is similar, there is a need to explore the results based on nonhyperbolic NMO as opposed to the standard hyperbolic NMO calculations.

## SEISMIC SURVEY ACQUISITION

On October 24$^{th}$, 2002, Devon Canada recorded a 3-C, 2D test line at Jackfish Thermal Heavy Oil Project, Alberta, a SAGD heavy oil field presently in the development phase and pre-steam injection. This seismic survey was acquired by using dynamite charges of 60, 125, and 250 grams in sequence along the seismic line, each with a hole depth of 10 meters. The seismic line is oriented north-south. The charge size used

for this study is 125 grams, and spaced at 22.5 m. There were gaps on the seismic line which created areas of lower fold on the resulting stacked seismic section. Multicomponent receivers were used, with a receiver spacing of 7.5 m.

When using a P-wave source to acquire multicomponent data, the components which are recorded at the 3-C geophone include the vertical, radial and transverse components (Figure 1). On Figure 1, the small black and blue arrows indicate the direction of particle motion, where the blue arrows indicate the P-SV particle motion. Make note that for P-SV component shot record, there is a change from positive to negative polarity across the shot. The conversion point for the P-P data is referred to as the common depth point (CDP), while the P-SV conversion point is called the common conversion point (CCP).

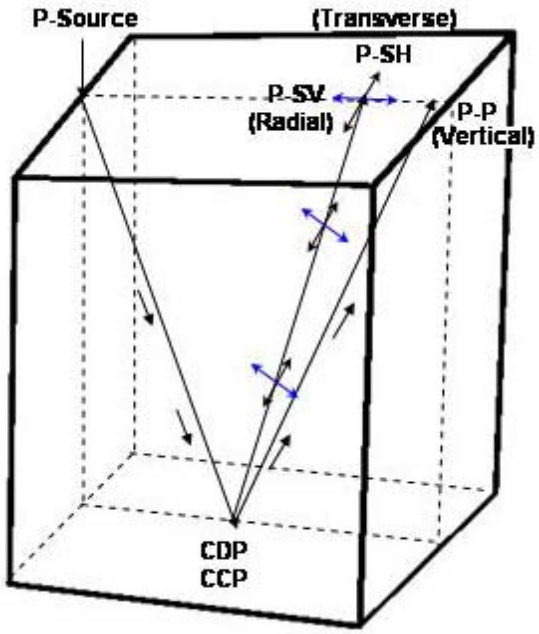


FIG. 1. Polarization vectors of a 3-C geophone using a P-source (modified from Tatham and McCormack, 1991).

In the Jackfish study area, the geology was initially assumed to be isotropic. As discussed by Tatham and McCormick (1991), the P-wave particle motion is confined to the source-receiver plane, therefore, the mode converted shear-wave particle motion must also be in this plane. Because the mode-converted P-S data is polarized in this way, each corresponding pair of traces from the horizontal components of the shot gather needed to be rotated into the source receiver plane (radial) and orthogonal plane (transverse) (Isaac, 1996). However, because this dataset consisted of a single 2D line with the radial component of the geophone already oriented along the source receiver plane, rotation of the horizontal components is not required. The azimuthal orientation of the geophone with respect to magnetic north was not thoroughly investigated and therefore, not corrected for.

## VERTICAL COMPONENT DATA PROCESSING

### Geometry

Shown in Figure 2 is the vertical component processing flow for the final migrated section. Before correcting the geometry, the raw shot records were divided into 3 separate lines, according to dynamite charge size. Using the 125 gram charge size, a -100 ms header static shift was first applied to compensate for the shift that was applied during VectorSeis acquisition. First breaks were calculated using Promax2D and exported to Hampson Russell GLI3D where the refraction statics where calculated. A 2-layer model was built in GLI3D and the refraction statics were imported into Promax2D, where the elevation corrections and refraction statics were applied to the time-shifted dataset. Elevation corrections were applied using a datum of 638.0 m, and a replacement velocity of 2000 m/s. The elevation profile for the Jackfish test line varies from 609.4 to 637.6 m, resulting in 28.2 m in elevation change along the two kilometre seismic line.

### Radial filter

The remaining vertical component processing flow was standard, once an effective noise attenuation and deconvolution method was found. Various noise attenuation and geometrical spreading methods were investigated, including TAR (true amplitude recovery), surface-wave attenuation, surface consistent amplitudes and radial filter. However, the radial filter was the only method that did not remove near-surface events or create a 'shadow zone' below the first breaks (Henley, 2003). Since the target reservoir is less than 500 m in depth the radial filter was ideal for removing low-frequency shot-generated linear noise. In Figure 3, the Devonian event is 'masked' by the low-frequency shot-generated noise. By applying a radial fan filter, the noise has been attenuated, leaving a continuous Devonian reflector on the near offset traces (Figure 4). Both the radial fan filter and dip filter were used to attenuate the linear noise. By using a minimum and maximum radial trace velocity of -2000 and 2000 m/s, respectively, velocities below these values are attenuated. From investigating the data that is being removed, there were no reflections being removed at or below and low frequencies of 10-15 Hz, and therefore 15 Hz was used as the low cut for this dataset. Similar parameters were used in the radial dip filter. Because there was still noise present at 2000 m/s and 600 m/s, these were removed by using a dip filter. A velocity range of 20 m/s was used on all dip filters, and applied in the frequency domain.

### Gabor Deconvolution

Gabor deconvolution was used because it was superior to conventional deconvolution processes for preserving the near-surface signal. Margrave, et al. (2003), has shown Gabor deconvolution to be superior at increasing the resolution of seismic data compared to traditional deconvolution processes in near-surface data. This superiority is due to the fact that Gabor deconvolution is a time-adaptive method as opposed to conventional methods which assume statistical stationarity.

Successful parameters include a half-width analysis window of 100 ms, with a window overlap of 2. The Burg spectrum used for wavelet estimation was Burg, with 10 coefficients and minimum phase, using hyperbolic time frequency smoother of 5 Hz-sec and window length of 10 Hz. A post-deconvolution filter was not applied during this

process. However, a high-pass filter does need to be applied prior to migration, due to Gabor whitening of noise in the input traces.

**Near surface static solution**

Both residual statics and trim statics were derived using Promax2D's external model correlation utility, which consists of four stages: model building, correlation computation, statics computation and statics application. The external modeling utility derives a static by cross-correlation of the individual traces sorted by CDP with the model. The trim statics were calculated in a similar way, however, the resulting static were applied directly to the channel static, whereas the residual statics were applied to CDP, shot and receiver static headers. Residual statics and velocity analysis were computed in an iterative fashion, where the final velocities for several CDP's indicated small lateral variations in stacking velocities along the line. The Devonian event is located between 400 and 500 ms.

The final stack was created using the updated velocity field, although, a significant amount of linear noise remained (Figure 6). When stacked without applying radial filter, events were contaminated with low frequency noise (Figure 5). With the radial filter applied, the low frequency noise has been attenuated, although, in some areas, such as the north end of the seismic line above the McMurray Formation, the radial filter appears to have removed signal. An Ormsby filter of 10-15-180-240 Hz, trace equalization, and a post-stack f-x deconvolution was applied to the final stack before migration.

**Kirchhoff migration**

The final stack was migrated with 15 degree dip aperture (Figure 7) using Kirchhoff time migration. Since the geology is relatively flat, the final stacked and migrated sections look similar, except for noise that was removed in the deeper part of the section below the Devonian event and along the edges of the data. The final migration with or without noise attenuation is almost identical, except for small areas where signal appears to lost when using the radial filter. For inversion, the f-x deconvolution was not applied, and therefore only the migration with the radial filter applied was used for inversion of the vertical component data.

Shown in Figures 8 and 9 are the frequency spectra for the raw shots and migrated sections, respectively. From raw shots, the frequency content varies considerably from shot to shot. Figure 8 indicates a frequency content of 10-20-70-90 Hz, whereas the frequency spectrum following migration indicates that the Gabor deconvolution operator is successfully boosting the amplitudes and flattening the frequency spectrum of the data as shown in Figure 9. In Figure 9 the low frequencies are constrained by the radial filter, however, there does appear to be frequencies up to 200 Hz.

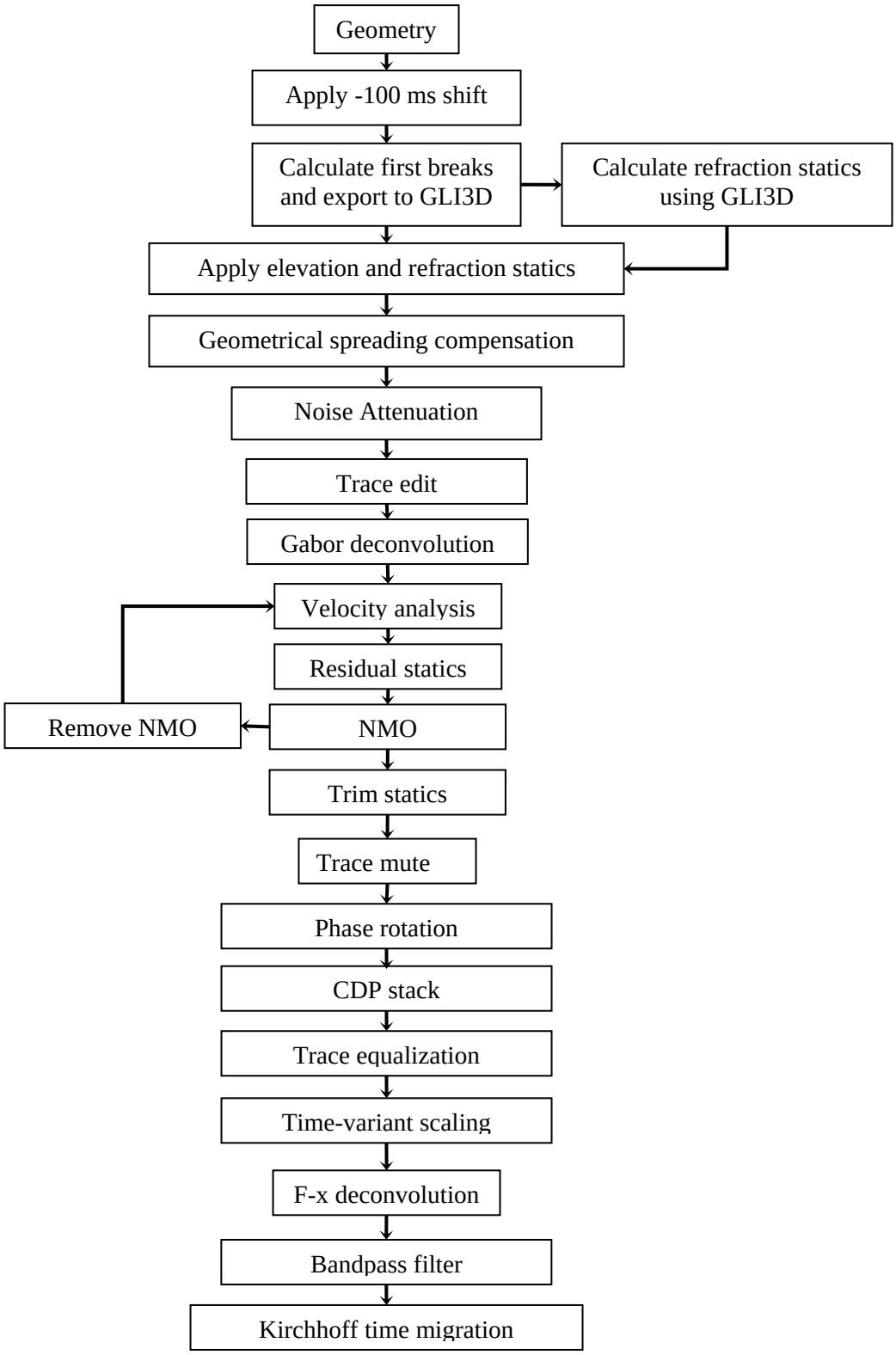


FIG. 2. Vertical component processing flow through to migration.

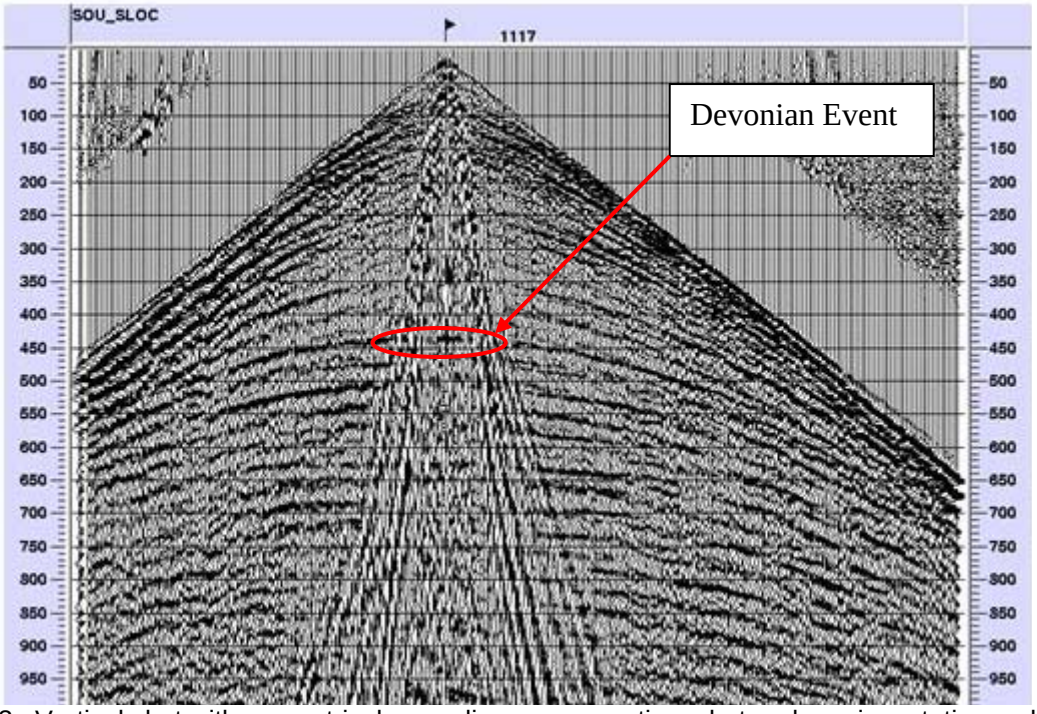


FIG. 3. Vertical shot with geometrical spreading compensation, shot and receiver statics and 5-8-180-240 Hz Ormsby filter.

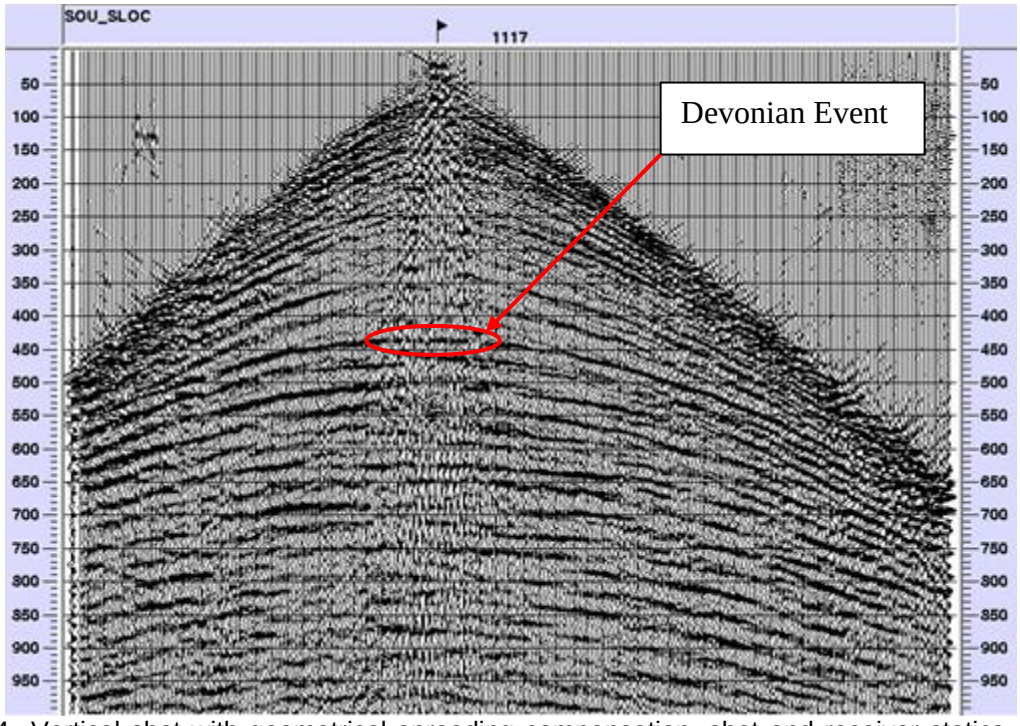


FIG. 4. Vertical shot with geometrical spreading compensation, shot and receiver statics, noise attenuation and 5-8-180-240 Hz Ormsby filter.

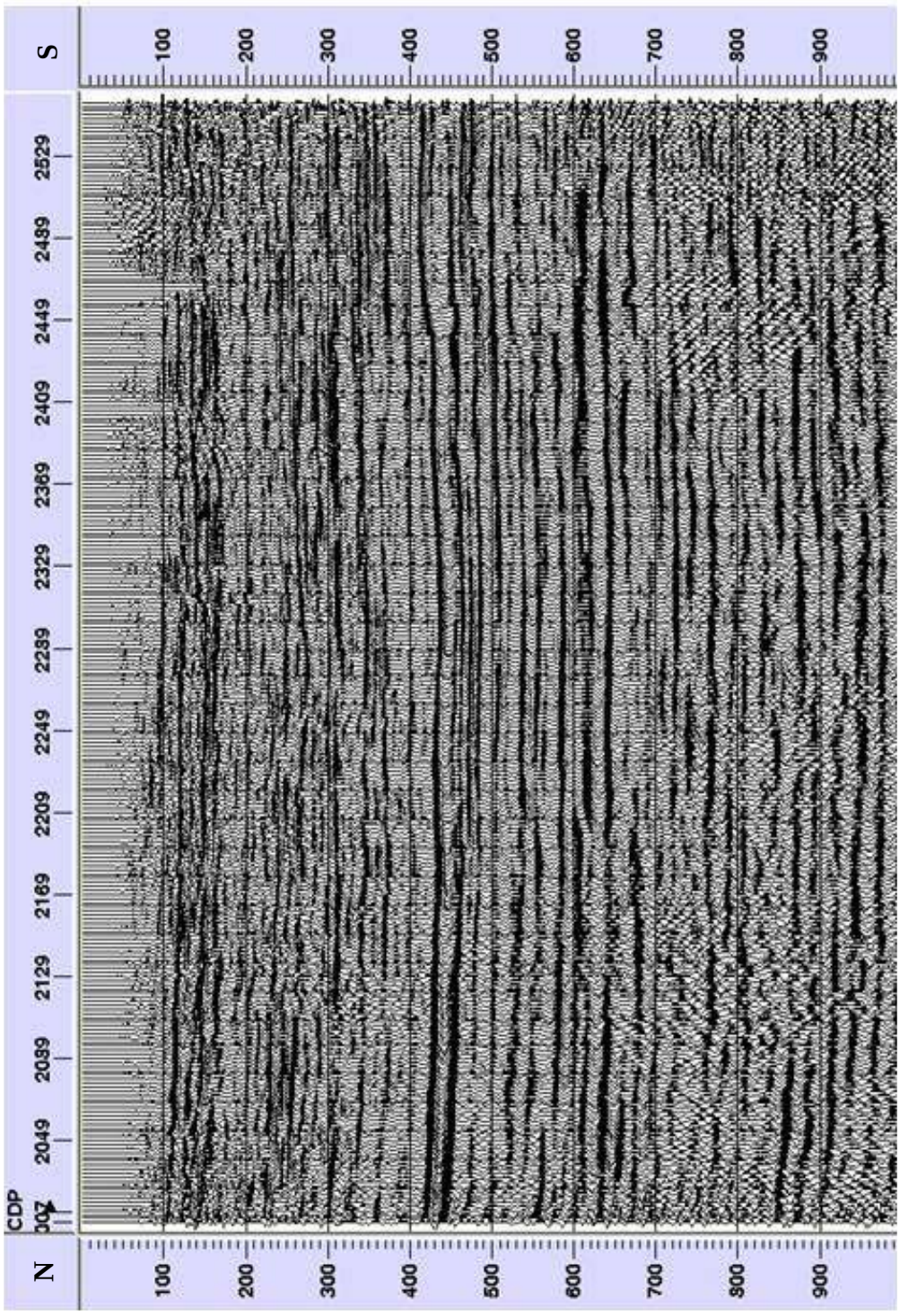


FIG. 5. Vertical component final stack with Gabor deconvolution and post stack 10-15-180-240 Hz Ormsby filter applied.

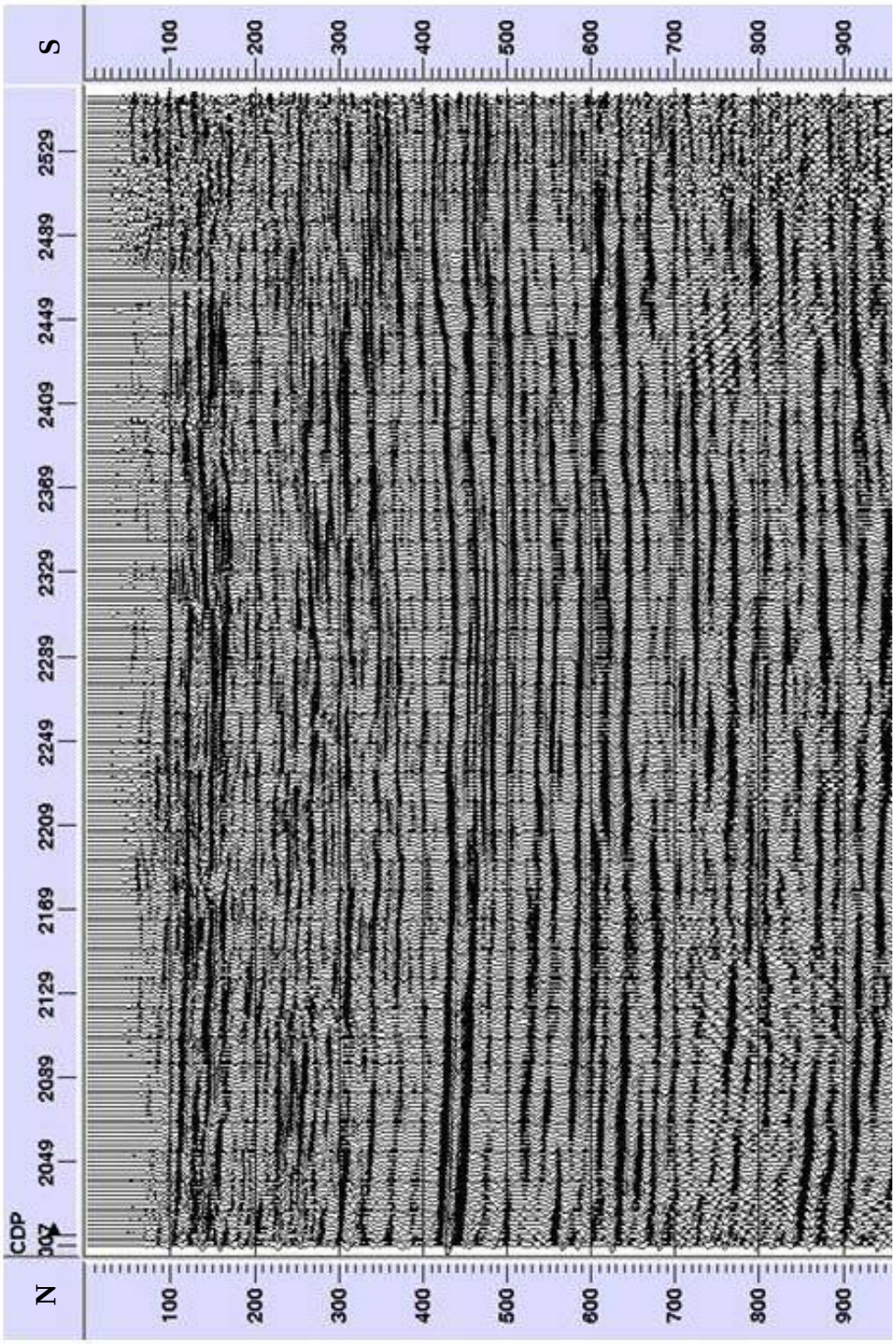


FIG. 6. Vertical component final stack with radial filter, Gabor deconvolution, and post stack 10-15-180-240 Hz Ormsby filter applied.

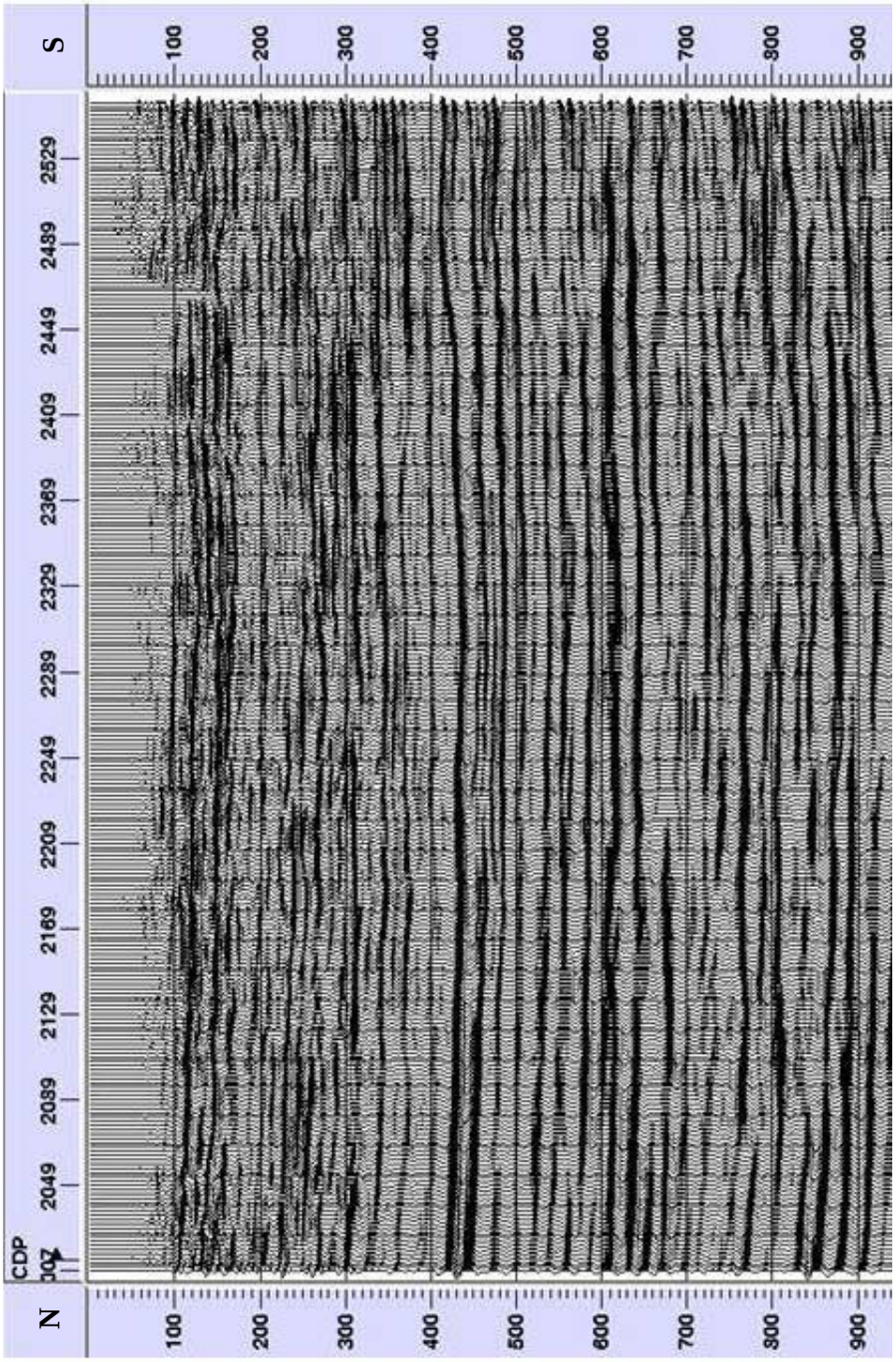


FIG. 7. Vertical component Kirchhoff time migration with radial filter, Gabor deconvolution and 10-15-180-240 Hz Ormsby filter applied before migration.

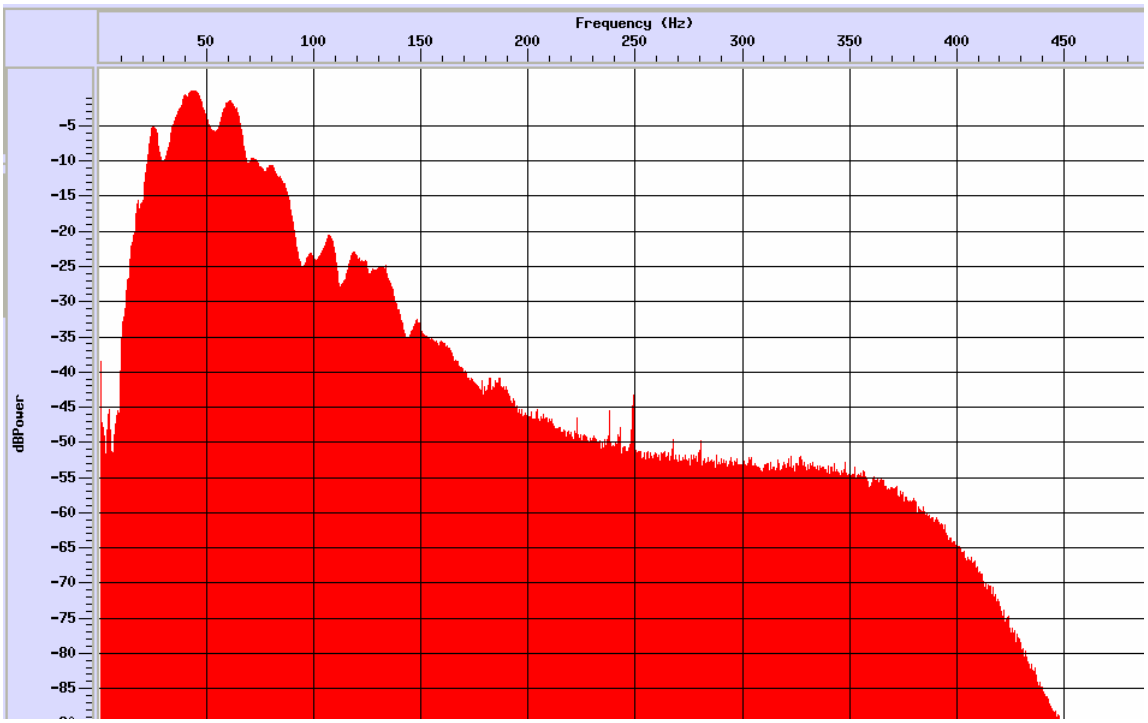


FIG. 8. Vertical component frequency spectrum of a typical shot record.

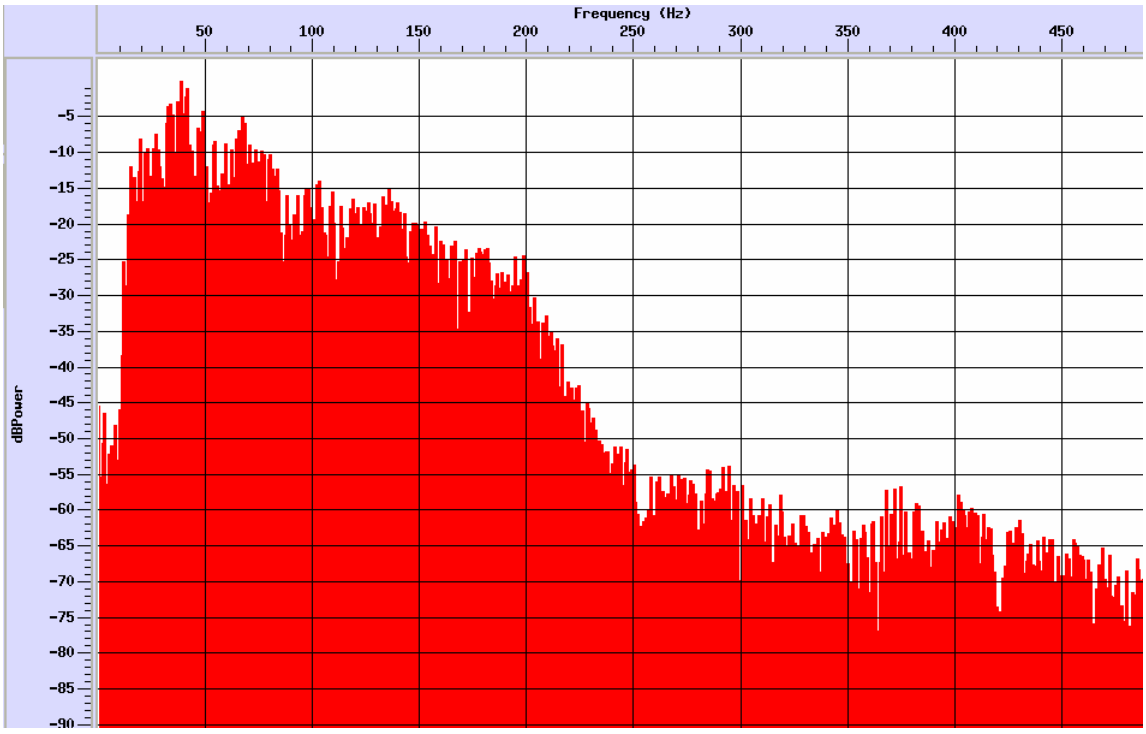


FIG. 9. Vertical component frequency spectrum following final migration.

## RADIAL COMPONENT DATA PROCESSING

As with many converted-wave processing flows, this dataset proved to be challenging to process because of large receiver statics and contamination of reflection data with shot-generated noise. The processing flow was based on established multicomponent processing flows created by Harrison (1992), Isaac (1996), and Lu and Hall (2003). The radial component processing flow was similar to the vertical component processing flow with some exceptions, which includes P-S asymptotic binning, polarity reversal, the calculation of receiver statics, and the incorporation of a depth-variant stack. The processing flow is shown in Figure 10, from initial geometry through to final migration. As discussed earlier, rotation of the horizontal components was not needed and therefore will not be included as part of the discussion about the radial component processing flow.

### Radial component geometry

Following the geometry assignment, common conversion point (CCP) binning using an asymptotic assumption was used to account for the asymmetry of the mode-converted ray path (Tessmer and Behle (1988); Behle and Dohr (1985). By using bins from the vertical component, both datasets will have identical CDP numbers, but, this is not the natural coordinate system of P-S data. In this process a Vp/Vs value needs to be estimated. In this case, a value of 2.2 was derived from well log data (Figure 11).

The polarity of the trailing spread traces was reversed, ensuring that all traces in the gather have identical P-S polarity. A 100 ms bulk shift was also applied to compensate for the shift applied to the VectorSeis data during acquisition. In order to calculate geometrical spreading compensation, an initial P-S velocity must first be calculated. The velocity table from P-P final stack was converted to P-S velocities using the following equation:

$$V_{ps} = \frac{V_{pp}}{\sqrt{V_p / V_s}} \tag{1}$$

where: $V_p$=P-P stacking velocity, $V_{ps}$=corresponding P-S stacking velocity, and Vp/Vs is the average velocity ratio.

This result is based on the result from Tessmer and Behle (1988) that the stacking velocity for P-S reflections is given by $\overline{V_{ps}} = \sqrt{V_p V_s}$ .

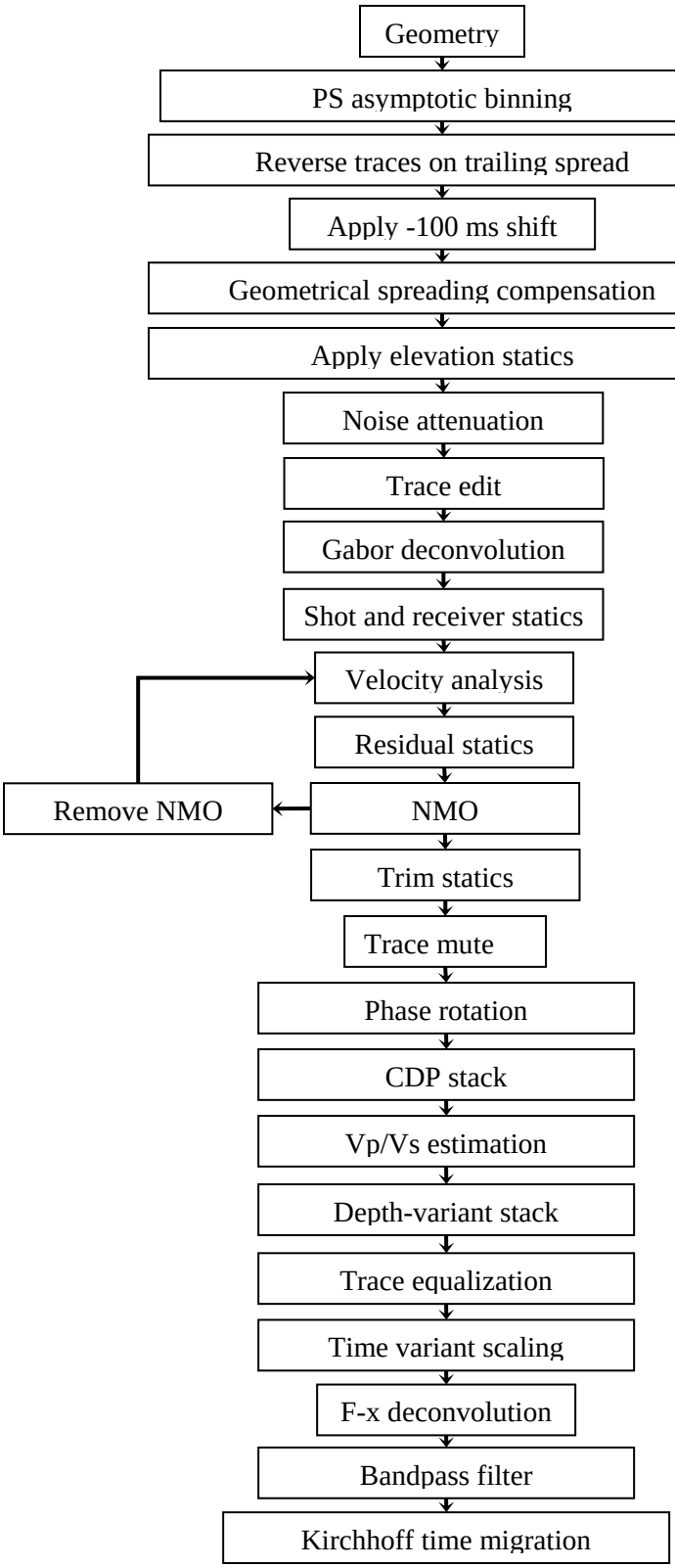


FIG. 10. Radial component processing flow through to migration.

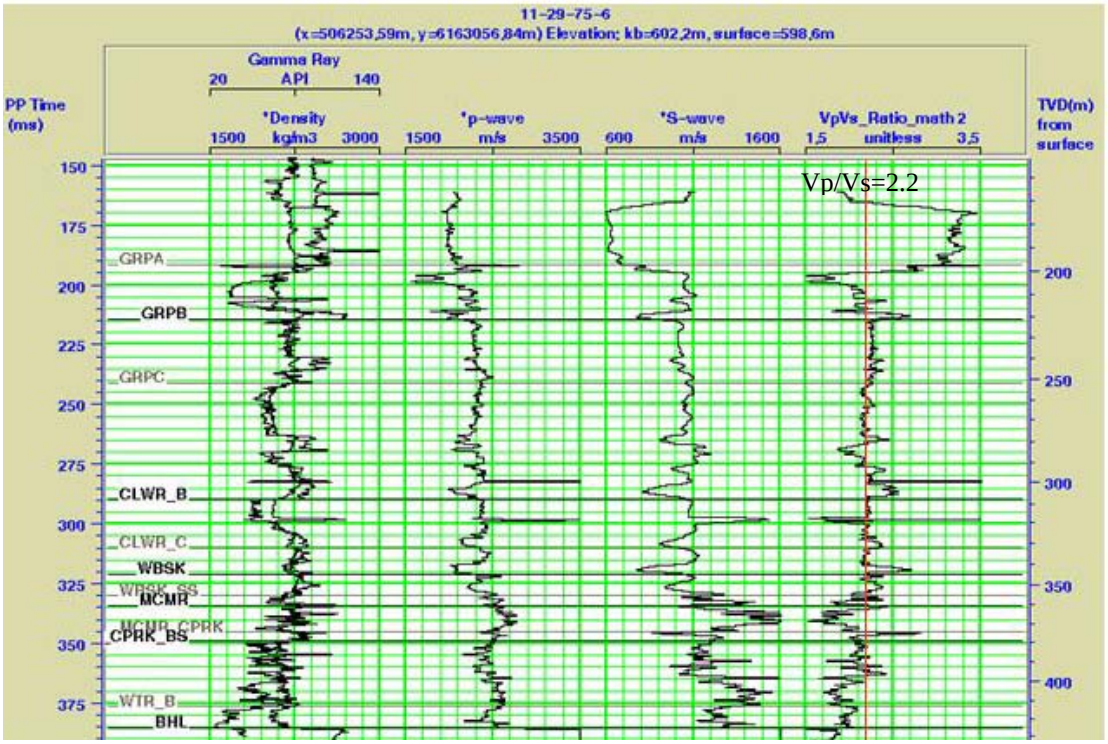


FIG. 11. Log display of dipole sonic well 11-29-75-6.

## Radial filter

Prior to calculating the receiver statics, the P-S reflections needed to be identified. To accomplish this, linear noise over the shallow part of the section was attenuated by applying a radial filter. One of the benefits of using the radial filter, designed by Dave Henley, is its ability to remove linear noise at various velocities, whether originating from one source or from several sources (Henley, 2003). After testing the radial filter, there do not appear to be events under the 8-12 Hz low pass bandwidth. Artefacts were removed in the data from the application of the radial filter by applying an additional iteration of the radial filter to remove backscatter remaining on the shot gathers.

The radial fan filter parameters were similar to those used for the vertical component with the exception of velocity where there was a second fan filter of +/- 400 m/s, with time coordinate of 0.4 s. Additionally, a filter was incorporated to remove backscatter for the first radial filter, which is placed at time coordinate of -1 s. Shown in Figures 12 and 13, are receiver gathers of the raw data before and after noise attenuation. The red oval on both figures shows the removal of low frequency noise, resulting in the appearance of a coherent event at 800-900 ms.

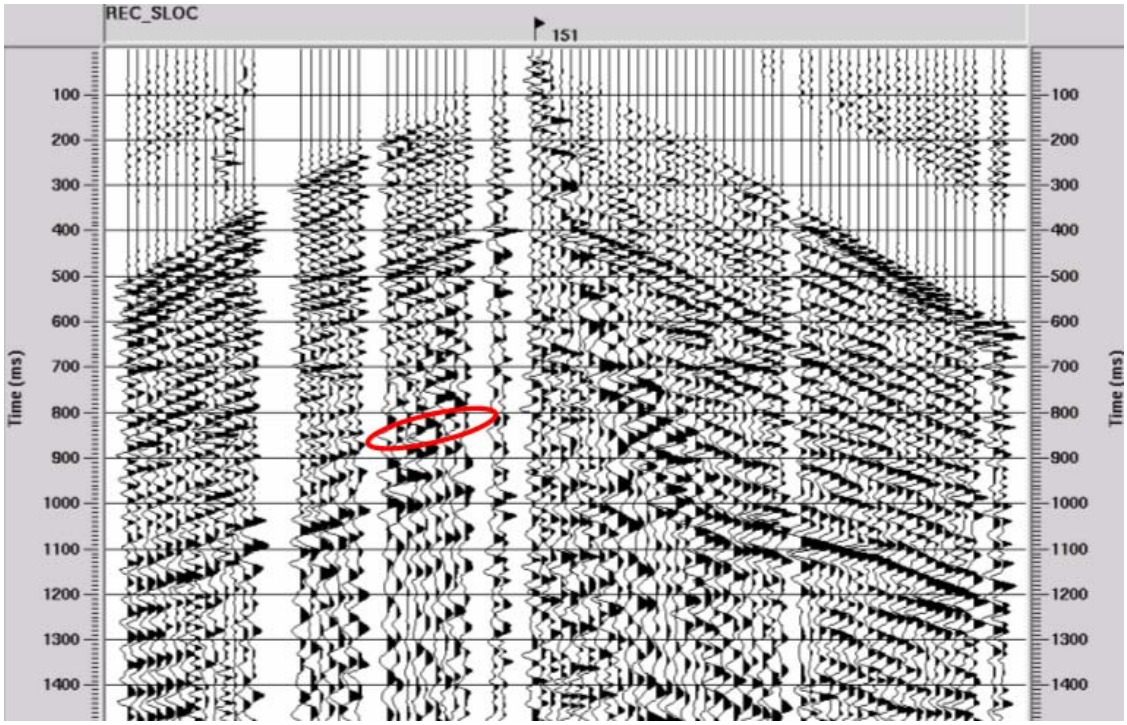


FIG. 12. P-S receiver gather with 8-12-50-60 Hz Ormsby filter and 500 ms AGC applied.

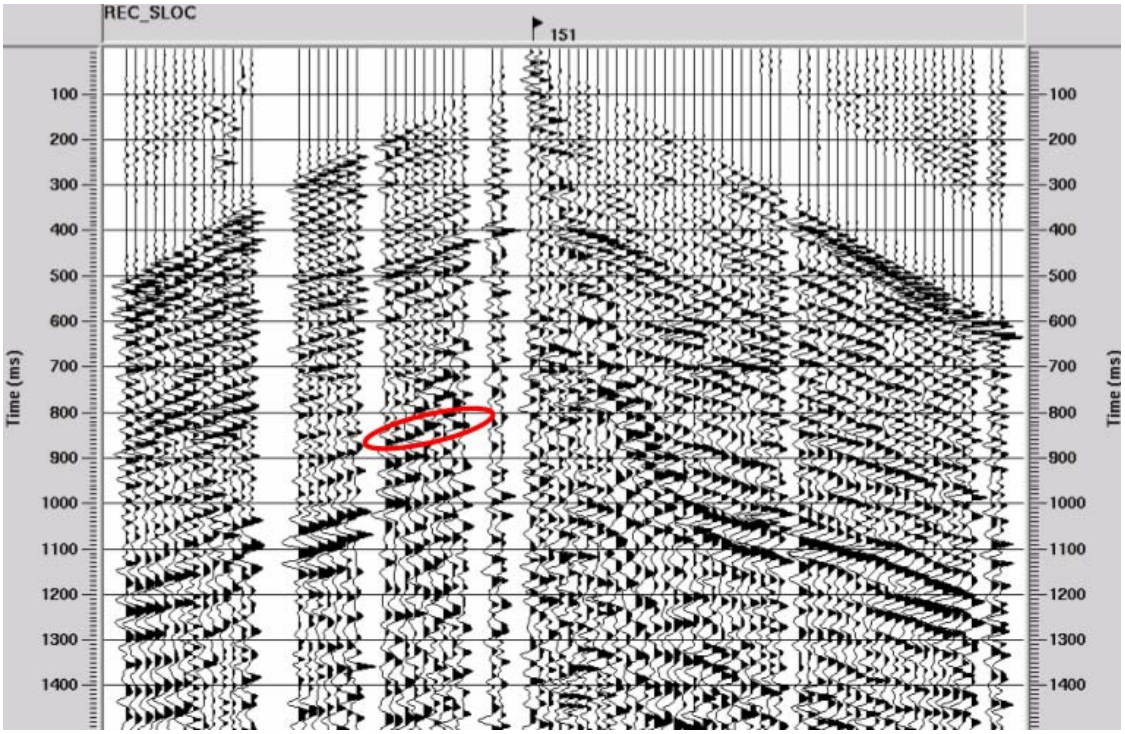


FIG. 13. P-S receiver gather with radial filter, 8-12-50-60 Hz Ormsby filter and 500 ms AGC applied.

## Gabor deconvolution

To enhance the signal to noise ratios and boost the frequency content of the seismic data, Gabor deconvolution was applied. Similar parameters were used as in the vertical component data, with the exception of the number of coefficients for the Burg spectrum, which were 5 as opposed to 10 in the vertical component. Results of Gabor deconvolution were favorable over conventional deconvolution processes at the either end of the seismic line, where there is low signal to noise and low fold. Shown in Figures 14-15 are the results of applying the radial filter and Gabor deconvolution to prestack data. The brute stack in Figure 14 contains significant amount of linear noise which is "masking" the reflections. By removing the linear noise and boosting the amplitudes, the Devonian event at 630 ms is now a continuous bright event on Figure 15.

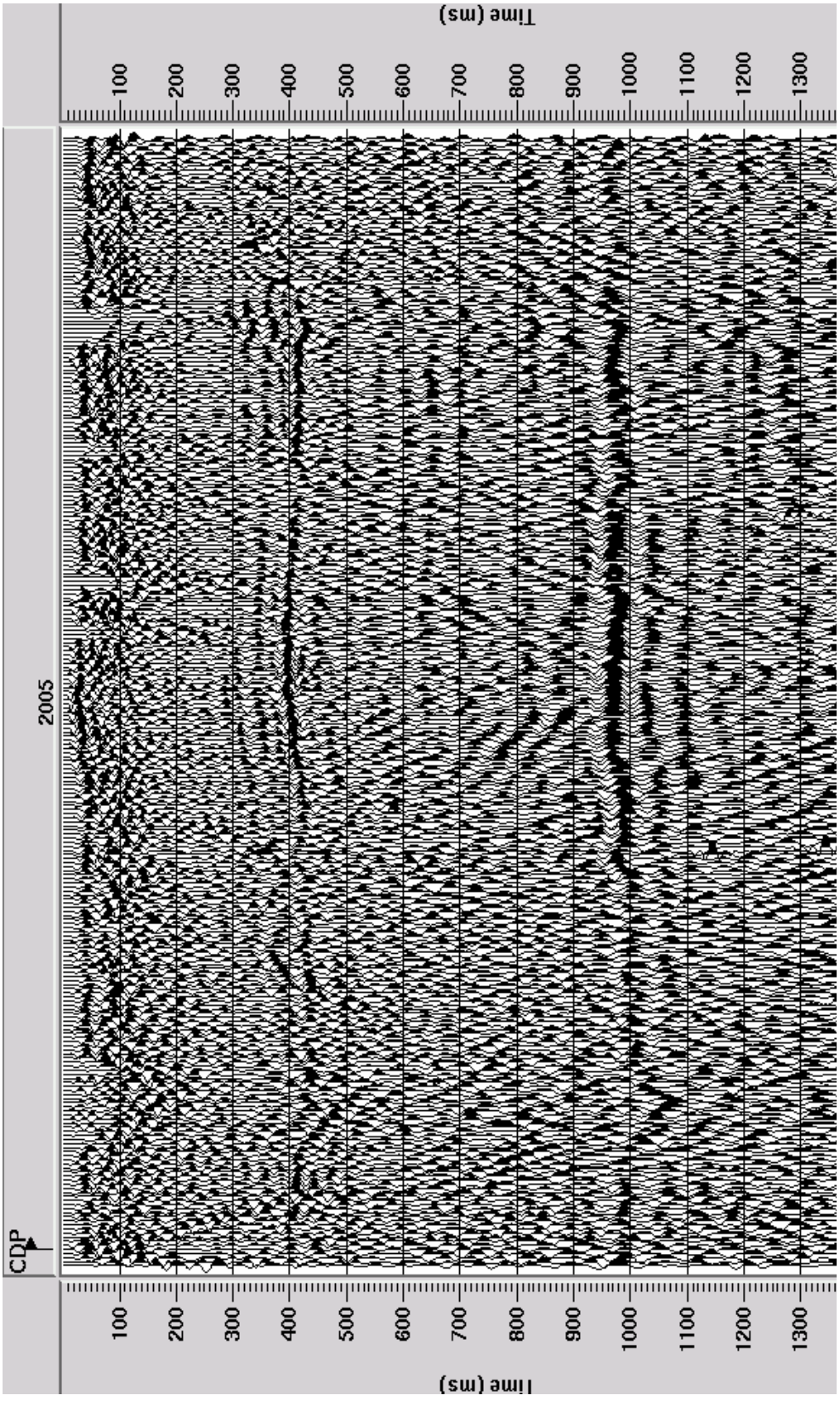


FIG. 14. Radial component brute stack with 8-12-50-60 Hz Ormsby filter and 200 ms AGC applied.

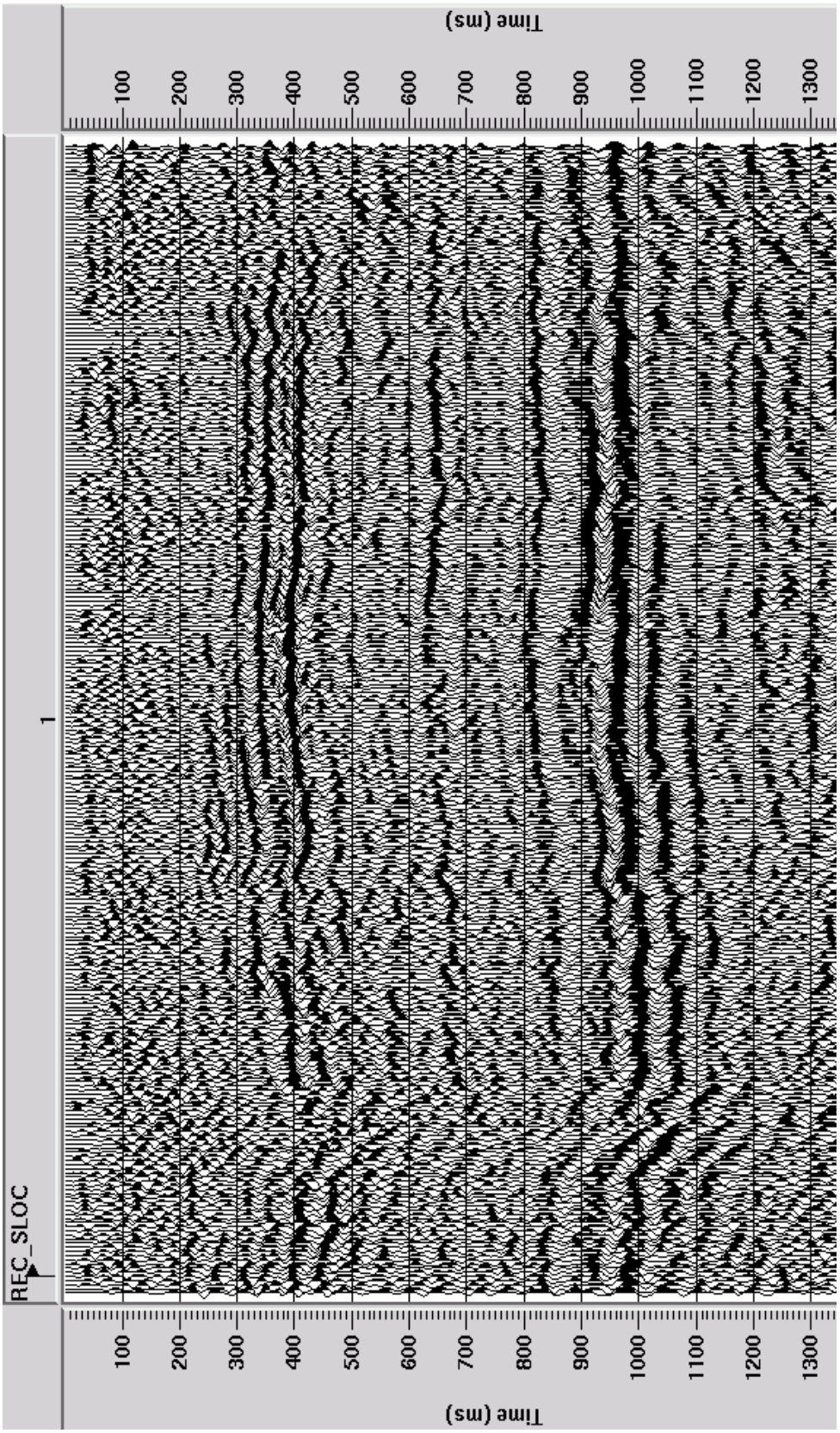


FIG. 15. Radial component brute stack with radial filter, 8-12-50-60 Hz Ormsby filter and 200 ms AGC applied.

**Near Surface Statics Solution**

For the converted wave data, shot statics were imported from the vertical component database. The shot statics should be identical for the P-P and P-S datasets, since the down going P-wave is the same for both components. As an initial estimate of receiver statics, the vertical component shot statics were multiplied by the average Vp/Vs of 2.2 and applied to the converted-wave data. However, large statics still remained on the receiver gathers, due to the slow up-going S-wave, and therefore additional static calculations needed to be implemented to calculate receiver statics.

The method used to calculate receiver statics includes sorting the P-S data into receiver gathers, apply NMO corrections and stack the data to create an initial brute stack. Because the receiver statics were large on the north end of the line, a commonly used method of calculating receiver statics by using auto-statics (Cary and Eaton, 1993), was not used. The method of hand statics used by Isaac (1996), which involved picking an event in the common receiver stack domain, flattening it and incorporating the static shift to the database. This procedure is only valid for flat reflectors. The reflector used in the hand static procedure, is the event which occurs around 1 second. Unfortunately, the Devonian event is not completely visible on the receiver stack. The remaining receiver static was removed through the residual autostatics procedure.

To calculate residual statics, the same method was used for the radial component as for the vertical component. Shots used for the residual statics had offsets of 100-1700 m, to remove the near offset noise in the shot gathers. The initial cross-correlation time gate was centered at the predicted Devonian event of 630 ms, at 300-960 ms, with an allowable static of 36 ms, and decreased by half with each iteration. The static applied at the third iteration was only +/-1 to 2 ms. However, the results of using the predicted P-S stacking velocities were not ideal, and therefore a stacking velocity using the P-S data need to be calculated. Because converted wave data is only hyperbolic for near offsets, hyperbolic and non-hyperbolic NMO equations were also tested. The standard 2-term NMO equation was used for the hyperbolic NMO estimation:

$$t^2 = t_0^2 + \frac{x^2}{v_{rms}^2} \quad \text{(Taner and Koehler, 1969)} \tag{2}$$

where: t =traveltime at x, $t_0$ = traveltime at zero offset, x =source-receiver offset, and $V_{rms}$ = RMS velocity which controls the moveout.

Tsvankin's long offset equation used for non-hyperbolic NMO, which uses the full 3 term equation with Taylor coefficients, valid for weak anisotropy:

$$t_A^2 \equiv t_0^2 + A_2 x^2 + \frac{A_4 x^4}{1 + A^* x^2} \quad \text{(Tsvankin and Thomsen, 1994)} \tag{3}$$

where: $t_0$ = traveltime at zero offset, $t_A$ =traveltime, $A^* = \frac{A_4}{\frac{1}{V_h^2} - A_2}$, and x = source-receiver offset.

Shot gathers using hyperbolic and nonhyperbolic NMO, are displayed in Figures 16-17 respectively and there does not appear to have an improved by using the nonhyperbolic NMO approximation. Therefore, hyperbolic NMO equation was used for the remainder of the processing. Residual static computation and velocity analysis were computed in an iterative fashion, followed by trim statics.

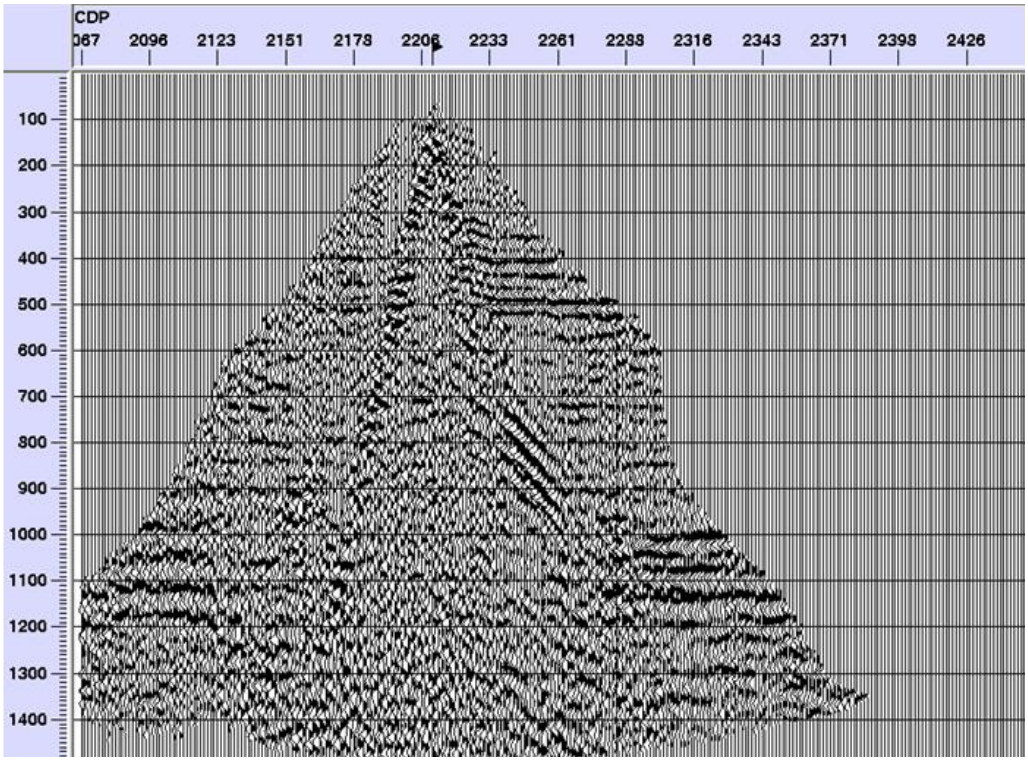


FIG. 16. P-S shot gather with hyperbolic NMO and 200 ms AGC applied.

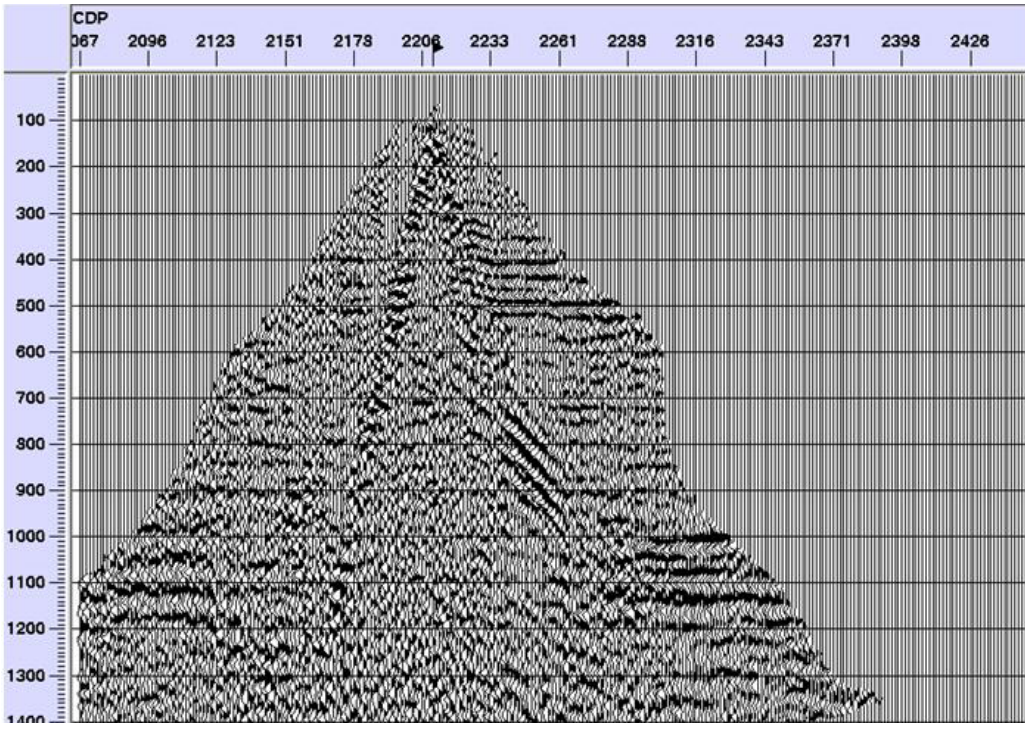


FIG. 17. P-S shot gather with non-hyperbolic NMO, and 200 ms AGC applied.

**Depth-variant stack**

One problem with velocity analysis is that near surface velocities are not pickable on the semblance plot. The depth-variant stack was introduced by Eaton et al. (1990), to correctly locate converted wave reflections and minimize some binning related artefacts. To complete a depth-variant stack, several Vp/Vs values must be calculated using the same horizons from the vertical and radial components. The Vp/Vs values are then calculated using the following equation from Harrison (1992):

$$\frac{Vp}{Vs} = \frac{2Is}{Ip} - 1 \qquad (4)$$

where: *Is* = time interval between P-S reflections and *Ip*=time interval between the P-P reflections.

For near-surface data above 300 ms, Vp/Vs values from logs were used in place of the preceding method. The depth-variant stack takes the calculated Vp/Vs values and the final vertical component velocity cube to create a converted-wave velocity cube. Because only one Vp/Vs value is used, the resulting velocities may not show lateral variations that are present on the radial component data, if the same variations are not present in the vertical component data. This can cause a decrease in resolution of the image of laterally varying reservoirs. In Figure 19, the depth-variant stack has successfully resolved the near-surface events. However, there is concern about preserving lateral variations. The final migrated section from the depth-variant stack is shown in Figure 20. The first 100 ms were removed from the top of the data due to removing the first 100 m of offset in my stacks.

Because heavy oil reservoirs have lateral variations in lithology and porosity, both stacks were migrated, although, the migrated depth-variant stack was used for inversion. The frequency spectrum for the raw data and after migration are shown in Figures 21 and 22, respectively. The bandwidth of the processed data is not as high as was expected (under 70 Hz), although, the deconvolution has broadened the amplitude spectrum, by enhancing the high frequency content.

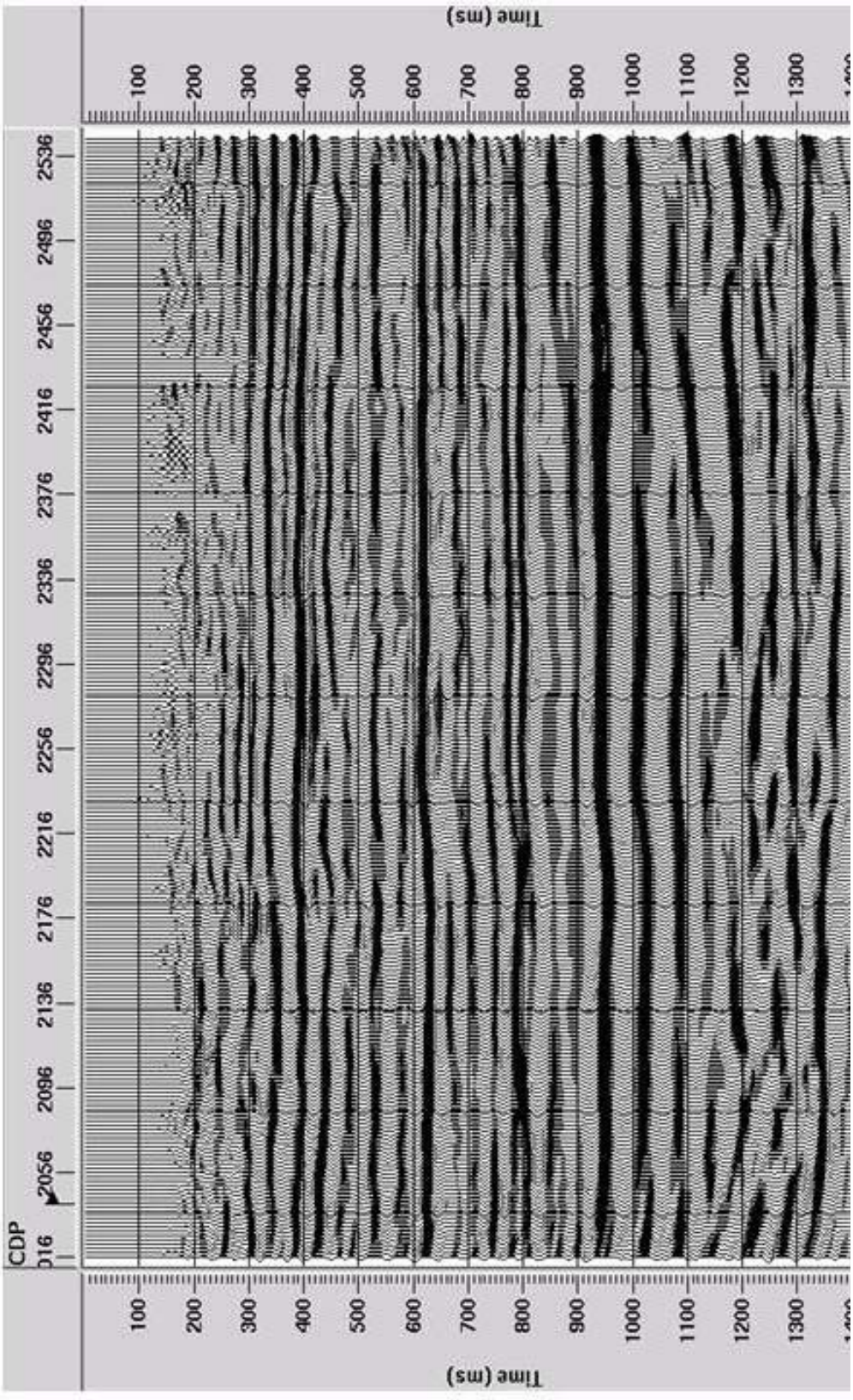


FIG. 18. Radial component Kirchhoff time migration from CDP stack, with radial filter, Gabor deconvolution, with 8-12-70-90 Hz Ormsby filter and 200 ms AGC applied.

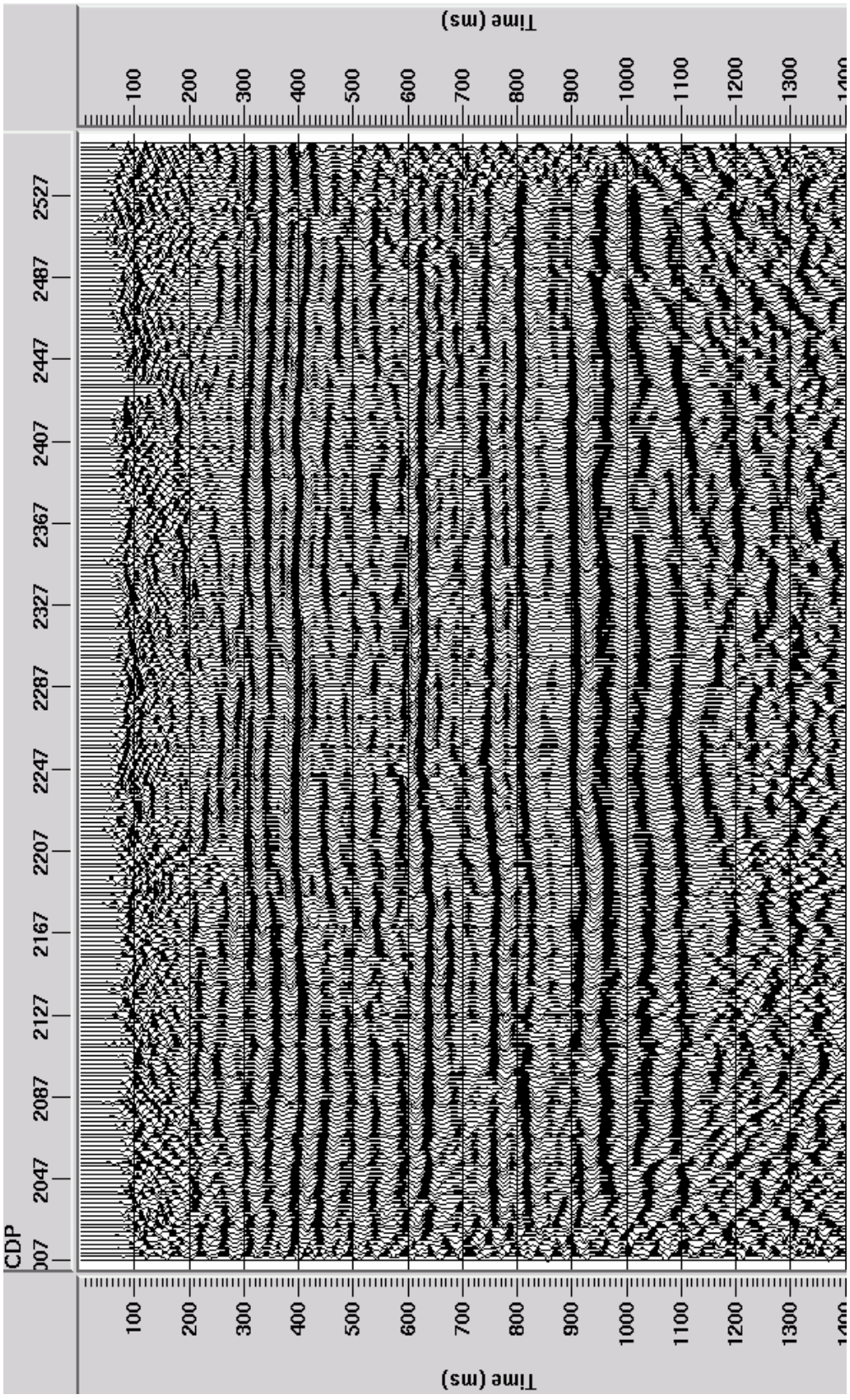


FIG. 19. Radial component depth-variant stack, with radial filter, Gabor deconvolution, 8-12-70-90 Hz Ormsby filter and 200 ms AGC applied.

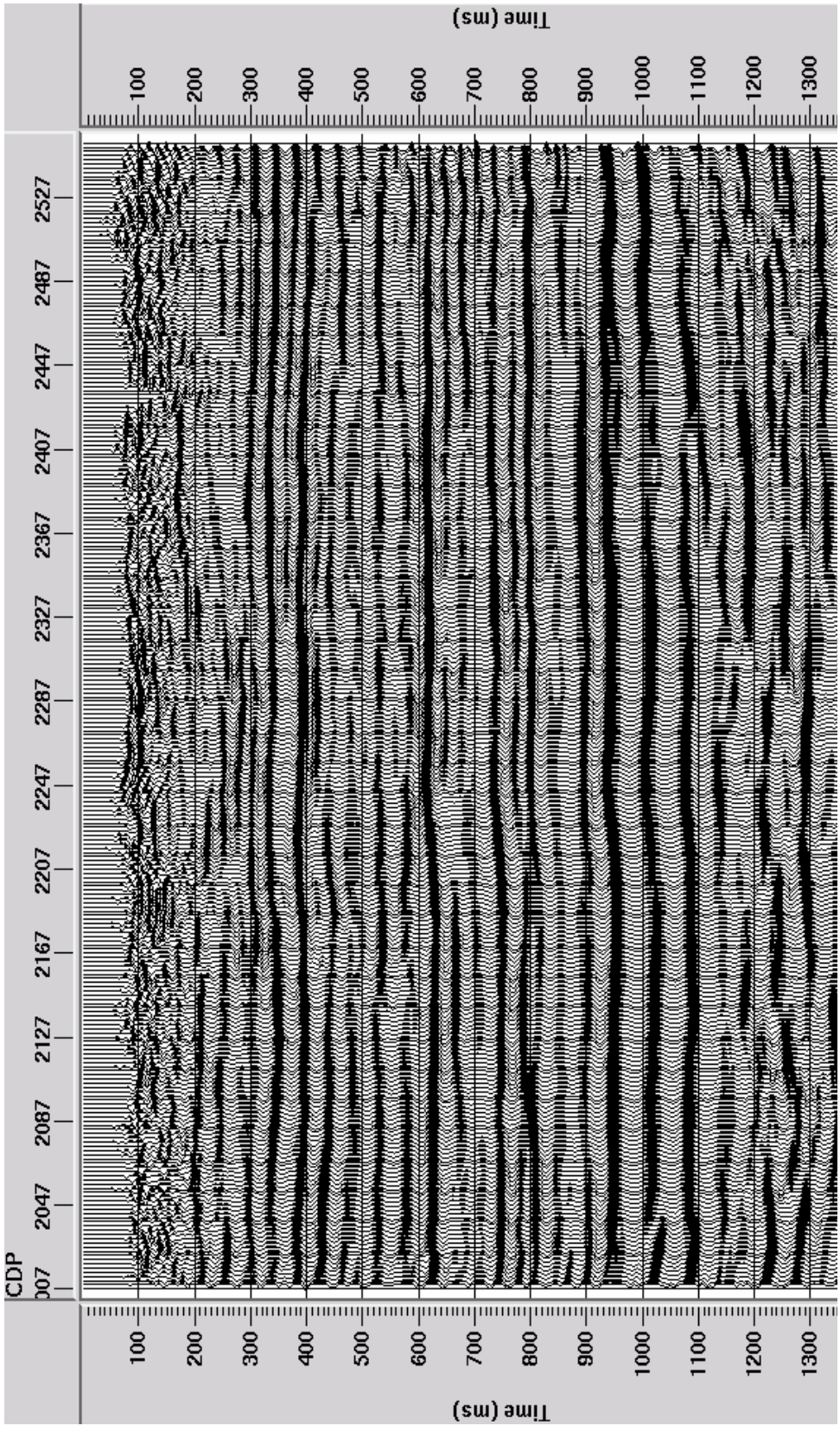


FIG. 20. Radial component Kirchhoff time migration from depth-variant stack, with radial filter, Gabor deconvolution, 8-12-70-90 Hz Ormsby filter and 200 ms AGC applied.

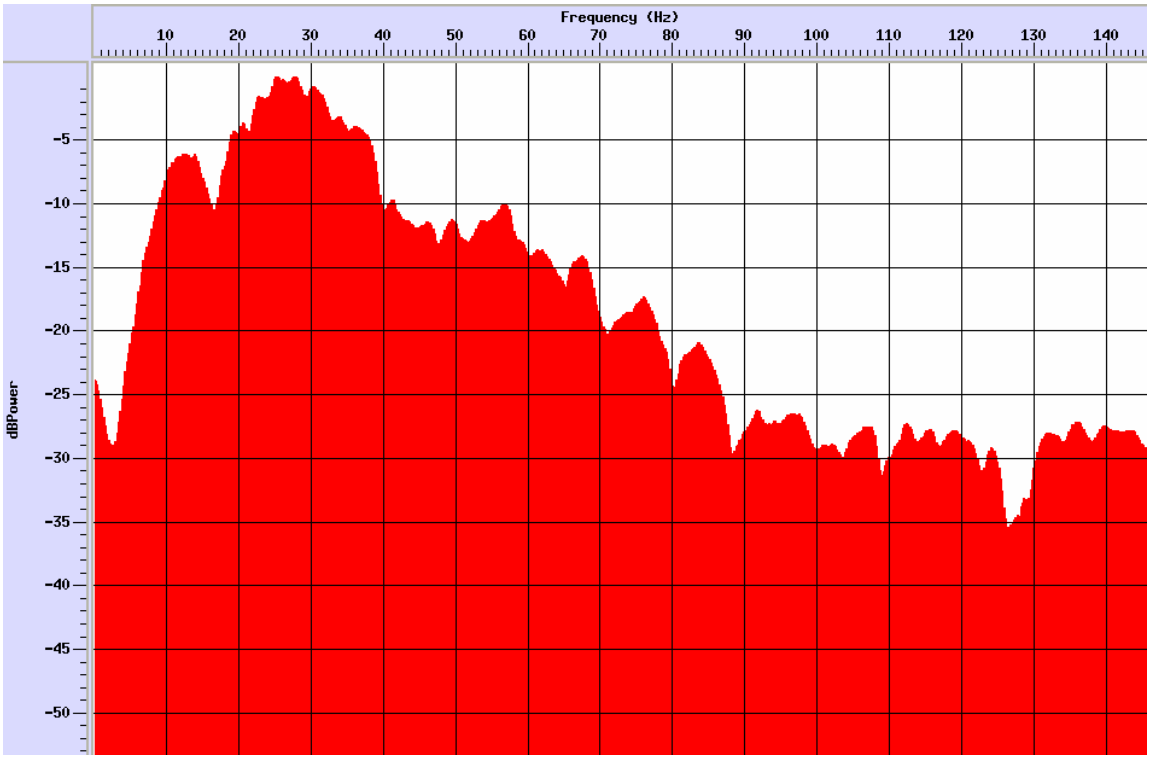


FIG. 21. Frequency spectrum for a typical raw shot.

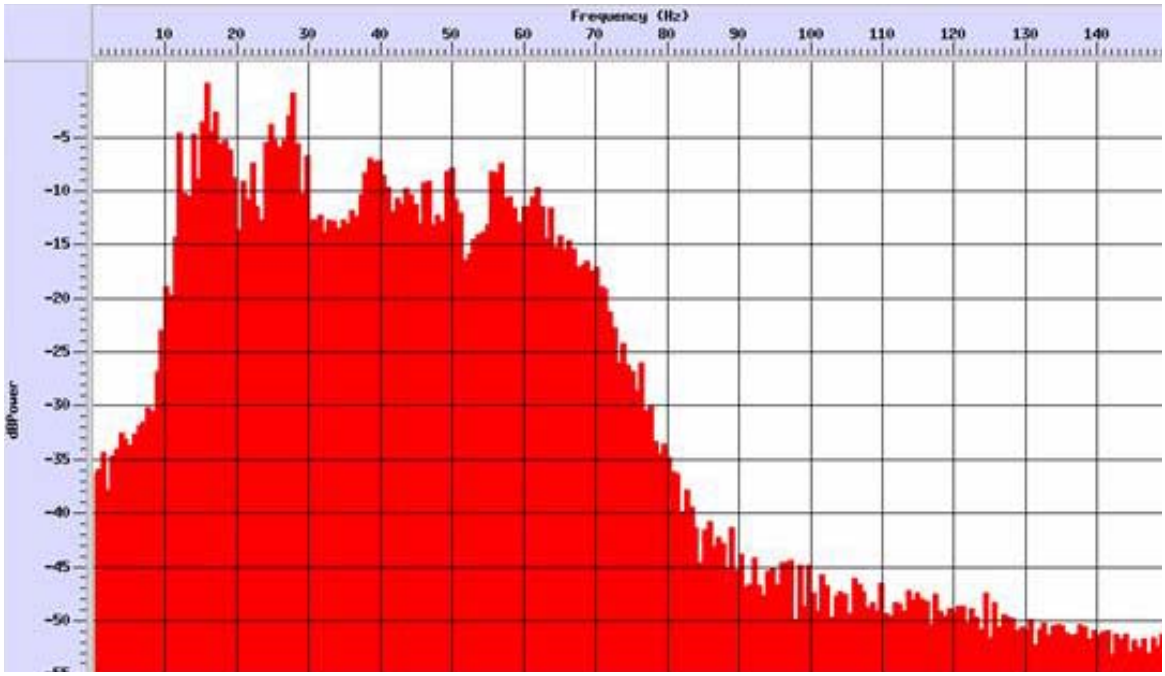


FIG. 22. Frequency spectrum for radial data following Kirchhoff migration.

## CONCLUSIONS

The final migrated section for the vertical component was the result of a standard processing flow. Particularly noteworthy is the result from using noise attenuation and removing noise attenuation filters yielded similar results when using f-x deconvolution prior to migration. For the radial component, the radial filter was found to remove a significant amount of linear noise in the shot gathers. Both the asymptotic and CCP stack and depth-variant stacks were migrated. The depth-variant stack may remove lateral variations in the velocity field, but has shown to have greater frequency in the near surface data. The CDP stack was found to have higher frequency and resolution for the deeper events below 700 ms.

## ACKNOWLEDGEMENTS

I would like to thank AICISE for funding this work, CREWES for technical support, and Landmark and Hampson Russell for donating software used to complete this project.

## REFERENCES

Al-Chalabi, M., 1973, Series approximation in velocity and travel time computations: Geophysical Prospecting, **21**, 783-795.

Alkhalifah, T., 1997, Velocity analysis using nonhyperbolic moveout in transversely isotropic media: Geophysics, **62**, 1839-1854.

Behle, A., and Dohr G., 1985, Converted waves in exploration seismics: in Dohr, G., ed., Seismic shear-waves: Part B: Applications, Geophysical Press, v. **15B**.

Cary P., and Eaton, D., 1993, A simple method for resolving large converted-wave (P-SV) statics. Geophysics, **58**, 429-433.

Castagna, J. and Chen, H., 2000, Anisotropy effects on full and partial stacks: Geophysics, **65**, 1028-1031.

Eaton, D.W.S., Slotboom, R.T., Stewart, R.R., and Lawton, D.C., 1990, Depth variant converted wave stacking: 60th SEG, Expanded Abstract, 1107-1110.

Harrison, M. P., 1992, Processing of P-SV surface seismic data: Anisotropy analysis, dip moveout and migration: Ph. D. thesis, University of Calgary, Department of Geology and Geophysics.

Henley, D., 2003, Coherent noise attenuation in the radial trace domain: Geophysics, **68**, 1408-1416.

Isaac, J. H., 1996, Seismic methods for heavy oil reservoir monitoring: Ph. D. thesis, University of Calgary, Department of Geology and Geophysics.

Iverson, W., Fahmy, B., and Smithson, S., 1989, VpVs from mode-converted P-S reflections: Geophysics, **54**, 843-852.

Lu H., and Hall, K., 2003, Tutorial: converted wave (2D PS) processing. CREWES Research Report, **15**.

Margrave, G, Dong, L., Gibson, P., Grossman, J., Henley, D., and Lamoureux, M., 2003, Gabor Deconvolution: extending Wiener's method to nonstationarity. CREWES Research Report, **15**.

Newrick, R., and Lawton, D., 2003, Investigation of turning rays in the Western Canada Sedimentary Basin: 2003 CSPG/CSEG Convention-Partners in a New Environment, Expanded Abstracts, CD ROM.

Taner M., and Koehler, F., 1969, Velocity spectra-digital computer derivation and applications of velocity functions. Geophysics, **34**, 859-881.

Tatham R., and McCormick, M., 1991, Multicomponent seismology in petroleum exploration: Society of Exploration Geophysicists.

Tessmer G., and Behle, A., 1988, Common Reflection point data-stacking technique for converted waves. Geophysical Prospecting, **36**, 671-688.

Tsvankin, I., and Thomsen, L., 1994, Nonhyperbolic reflection moveout in anisotropic media: Geophysics, **59**, 1290-1304.